PROCEEDINGS OF SCIENCE

Measurements of the Higgs Boson Mass and Couplings with ATLAS 13 TeV Data

Eric Feng[*†]
CERN
CH-1211
Geneva 23, Switzerland
E-mail: Eric.Feng@cern.ch

Combined measurements of the Higgs boson mass, as well as of its production times decay rates, are performed using the $H \to \gamma\gamma$ and $H \to ZZ^* \to 4\ell$ decay channels. The measurements are based on 36.1 fb^{-1} of proton–proton collision data recorded by the ATLAS experiment at the LHC at $\sqrt{s} = 13$ TeV. The Higgs boson mass is measured to be $124.98 \pm 0.19\,(\text{stat}) \pm 0.21\,(\text{syst})$ GeV. The rates for gluon fusion, vector-boson fusion, VH, and ttH production, as well as kinematic subdivisions of these processes, are found to be compatible with the Standard Model. The measured ratios of the Higgs boson couplings to their SM predictions are also consistent with the predictions.

ATL-PHYS-PROC-2017-228
25 October 2017

The European Physical Society Conference on High Energy Physics
5-12 July, 2017
Venice

[*]Speaker.
[†]On behalf of the ATLAS Collaboration

PoS(EPS-HEP2017)697

1. Data analysis

This contribution presents the combination of measurements of the Higgs boson mass and production times decay rates in the $H \to \gamma\gamma$ [1] and $H \to ZZ^* \to 4\ell$ ($\ell = e$ or μ) [2] decay channels, using proton–proton collision data corresponding to an integrated luminosity of 36.1 fb^{-1} produced by the LHC at a centre-of-mass energy of $\sqrt{s} = 13$ TeV and recorded by the ATLAS detector [3, 4] during 2015 and 2016. The full results are described in Refs. [5] and [6].

The measurements are based on preliminary calibrations for muons, electrons, and photons. Common nuisance parameters are used in all categories of both decay channels for shared sources of experimental and theoretical uncertainty.

2. Higgs boson mass

The Higgs boson mass has been measured using a combined fit to the invariant mass spectra of the decay channels $H \to ZZ^* \to 4\ell$ and $H \to \gamma\gamma$. A profile likelihood ratio is employed, treating the signal strengths as independent nuisance parameters. The sources of correlated systematic uncertainty include the calibrations of electrons, photons, the pileup modelling, and the luminosity.

The results from each of the individual channels and their combination, along with the combined fit to the ATLAS and CMS Run 1 data [7], are summarized in Figure 1. The combined mass measured is in excellent agreement with, and has similar statistical precision to, the LHC Run 1 measurement.

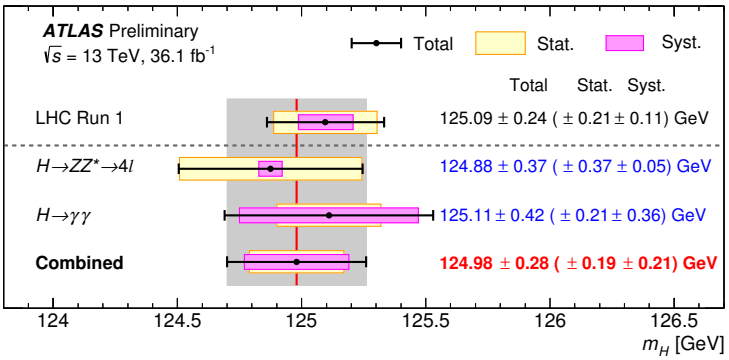

Figure 1: Summary of the Higgs boson mass measurements from the individual and combined analyses performed here, compared to the combined Run 1 measurement by ATLAS and CMS. Plot is taken from Ref. [5].

3. Higgs boson production

The measured events in each decay channel are separated into exclusive kinematic and topological categories. The categories are chosen to approximately match those of the simplified template cross-section regions [8]. The regions separate gluon-fusion production into bins of jet multiplicity and Higgs transverse momentum p_{T}^{H}, and into two bins in a vector boson fusion (VBF) topological region. Quark-initiated production processes are split into two VBF topological bins,

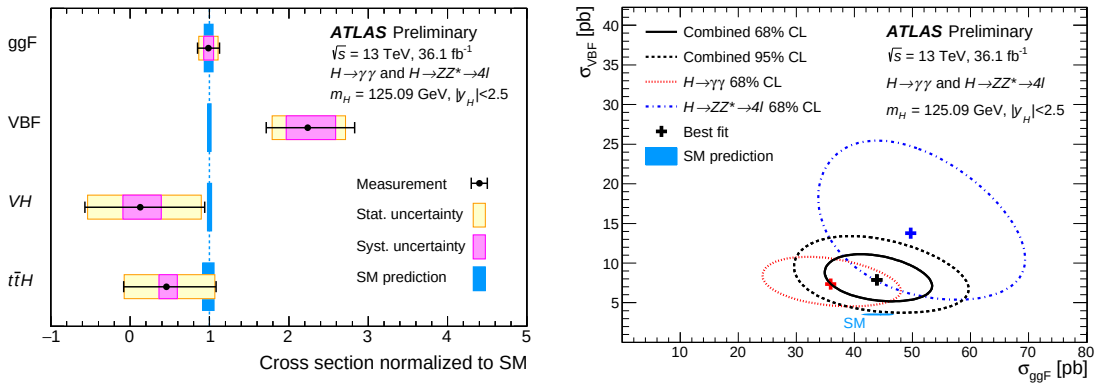

(a) (b)

Figure 2: (a) Cross sections for ggF, VBF, VH, and $t\bar{t}H$ normalized to the SM predictions and measured with the assumption of SM branching fractions. (b) Measured likelihood contours in the σ_{VBF} versus σ_{ggF} plane. The branching fractions are fixed to their SM values. Plots are taken from Ref. [6].

a VH bin with the vector boson decaying hadronically, and a bin for the remaining events. Finally, leptonic decays of the vector boson in VH production are split into the WH and ZH processes, and further split by the Higgs-boson p_{T}. The coupling measurements are performed assuming a Higgs boson mass of $125.09 \pm 0.21\,(\mathrm{stat.}) \pm 0.11\,(\mathrm{syst.})$ GeV [7].

The global signal strength μ is defined as the ratio of the observed yield to its Standard Model (SM) expectation. It is measured to be $\mu = 1.09 \pm 0.12 = 1.09 \pm 0.09\,(\mathrm{stat.})\,^{+0.06}_{-0.05}\,(\mathrm{exp.})\,^{+0.06}_{-0.05}\,(\mathrm{th.})$, which is consistent with the SM with a p-value of 47%. The leading uncertainties arise from missing higher-order terms in the perturbative calculation, as well as the luminosity.

The measured production cross sections of ggF, VBF, VH, and $t\bar{t}H$ for $|y_H| < 2.5$ and assuming SM branching fractions are shown in Figure 2(a). The four-dimensional compatibility with the SM prediction is 5%. Figure 2(b) shows the measured likelihood contours in the σ_{VBF} versus σ_{ggF} plane from $H \to \gamma\gamma$ and $H \to ZZ^* \to 4\ell$, and their combination, where the cross sections for VH and $t\bar{t}H$ are profiled with the data. The two-dimensional compatibility with the SM prediction is 3%.

The simplified template cross section framework defines a set of kinematic regions for each production process and combines these with the ratios of branching fractions for the various decay channels in order to probe the properties of the Higgs boson. For each production region i and decay mode f, the SM prediction $(\sigma_i \cdot \mathrm{B}_f)_{\mathrm{SM}}$ provides a template. The measured yields in the 31 $H \to \gamma\gamma$ categories and the 9 $H \to ZZ^* \to 4\ell$ categories, along with the corresponding detector acceptance and response, are used to extract the observed cross section in each region times B_{4l}, along with the ratio $\mathrm{B}_{\gamma\gamma}/\mathrm{B}_{4l}$.

The measurements reported here are the first ones towards stage 1 of the framework, which adds kinematic divisions, with Higgs-boson rapidity y_H satisfying $|y_H| < 2.5$. Lower-rate regions are merged in order to give sensitivity to SM production and to minimize correlations. The results in Figure 3 show good overall agreement with the SM predictions. The ten-dimensional compatibility

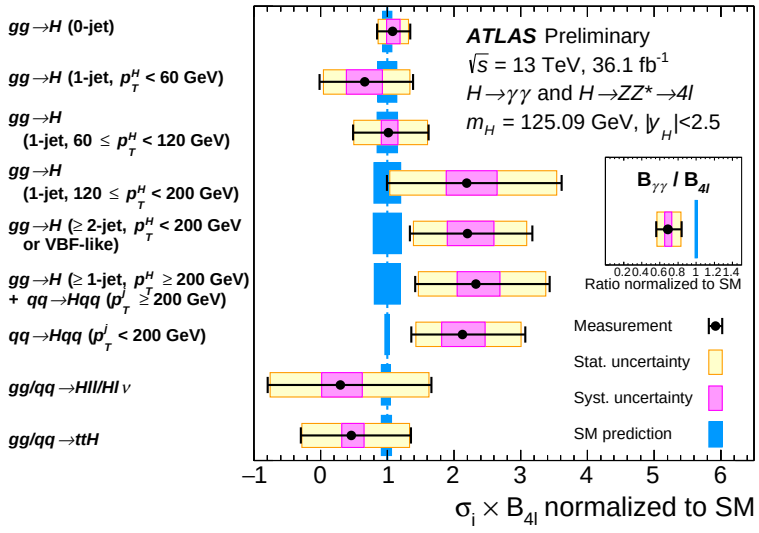

Figure 3: Cross section times B_{4l} measured in each of nine simplified template cross-section measurement regions, along with the measured ratio of branching fractions $B_{\gamma\gamma}/B_{4l}$. The results are normalized to the corresponding SM predictions. Plot is taken from Ref. [6].

with the SM prediction is 9%.

4. Higgs boson couplings

The κ framework parameterizes new Higgs boson interactions as multiplicative coefficients to cross sections and partial widths as follows [9]:

$$\sigma(i \to H \to f) = \kappa_i^2 \sigma_i^{\mathrm{SM}} \frac{\kappa_f^2 \Gamma_f^{\mathrm{SM}}}{\kappa_H^2 \Gamma_H^{\mathrm{SM}}}, \tag{4.1}$$

where i and f are the initial and final states, σ_i^{SM} is the SM production cross section, and Γ_H^{SM} and Γ_f^{SM} are the SM values of the total Higgs boson width and the partial width of final state f, respectively. In the results here the branching fraction to non-SM particles is assumed to be zero.

First a two-parameter fit is performed for common coefficients of couplings to fermions (κ_f) and to weak vector bosons (κ_V). The result in Figure 4(a) shows a positive correlation of 54% due in part to the destructive interference between the top-quark and W-boson loops in the $H \to \gamma\gamma$ decay. The best-fit values and uncertainties are $\kappa_V = 1.03 \pm 0.06$, $\kappa_f = 0.89^{+0.20}_{-0.15}$. The two-dimensional compatibility with the SM prediction is 52%.

In a separate model, the effective coefficients κ_g and κ_γ capture all potential loop contributions to the Higgs-boson interactions with gluons and photons, respectively. Here, production and decay modes other than ggF, $H \to gg$ and $H \to \gamma\gamma$ are fixed to their SM expectations. In Figure 4(b), the two-parameter fit for κ_g and κ_γ shows an anti-correlation of -64% because the leading constraint comes from $H \to \gamma\gamma$ in the gluon fusion channel. The best-fit values and uncertainties are $\kappa_g = 1.08^{+0.11}_{-0.10}$ and $\kappa_\gamma = 0.93^{+0.09}_{-0.08}$. The two-dimensional compatibility with the SM prediction is 68%.

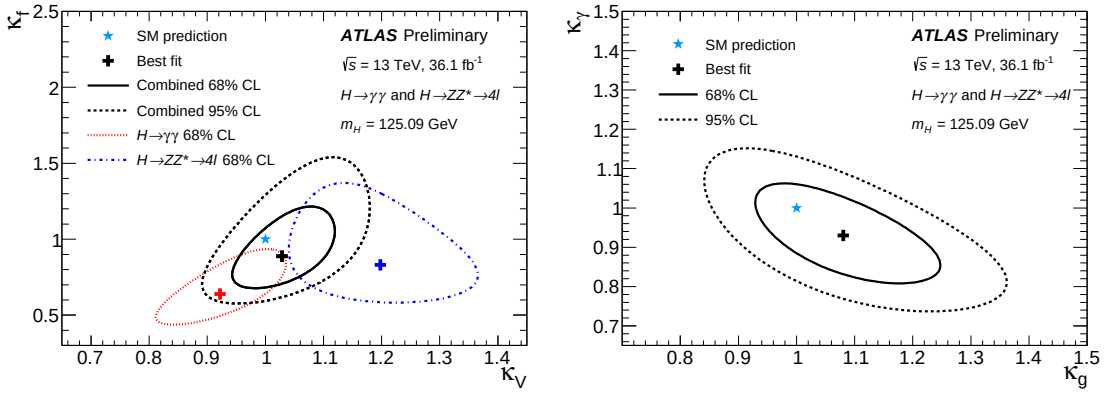

(a) (b)

Figure 4: (a) Contours at 68% and 95% CL in the (κ_F, κ_V) plane, and (b) contours at 68% and 95% CL in the (κ_γ, κ_g) plane. Plots are taken from Ref. [6].

References

[1] The ATLAS Collaboration, *Measurement of fiducial, differential and production cross sections in the $H \to \gamma\gamma$ decay channel with 20.3 fb^{-1} of 13 TeV pp collision data*, *ATLAS-CONF-2017-045* (2017).

[2] The ATLAS Collaboration, *Measurement of inclusive and differential cross sections in the $H \to ZZ^* \to 4\ell$ decay channel at 13 TeV with the ATLAS detector*, *ATLAS-CONF-2017-032* (2017).

[3] ATLAS Collaboration, *The ATLAS Experiment at the CERN Large Hadron Collider*, *JINST* **3** (2008) S08003.

[4] M. Capeans et al., *ATLAS Insertable B-layer Technical Design Report*, *CERN-LHCC-2010-013, ATLAS-TDR-19* (2010).

[5] ATLAS Collaboration, *Measurement of the Higgs boson mass in the $H \to ZZ^* \to 4\ell$ and $H \to \gamma\gamma$ channels with $\sqrt{s}$=13 TeV pp collisions using the ATLAS detector*, *ATLAS-CONF-2017-046* (2017).

[6] ATLAS Collaboration, *Combined measurements of Higgs boson production and decay in the $H \to ZZ^* \to 4\ell$ and $H \to \gamma\gamma$ channels using $\sqrt{s} = 13$ TeV pp collision data collected with the ATLAS experiment*, *ATLAS-CONF-2017-047* (2017).

[7] ATLAS and CMS Collaborations, *Combined Measurement of the Higgs Boson Mass in pp Collisions at $\sqrt{s} = 7$ and 8 TeV with the ATLAS and CMS Experiments*, *Phys. Rev. Lett.* **114** (2015) 191803, [arXiv:1503.0758].

[8] LHC Higgs Cross Section Working Group, *Handbook of LHC Higgs Cross Sections: 4. Deciphering the Nature of the Higgs Sector*, *CERN-2017-002-M* (2016) [arXiv:1610.0792].

[9] LHC Higgs Cross Section Working Group, *Handbook of LHC Higgs Cross Sections: 3. Higgs Properties*, *CERN-2013-004* (2013) [arXiv:1307.1347].